Available online at www.sciencedirect.com
SCIENCE DIRECT®
Journal of Power Sources 158 (2006) 518–523
JOURNAL OF POWER SOURCES
www.elsevier.com/locate/jpowsour

Structural and electrochemical properties of nanocrystalline $Li_xMn_2O_4$ thin film cathodes ($x = 1.0$–1.4)

S.R. Das [a], Istevao R. Fachini [b], S.B. Majumder [a], R.S. Katiyar [a,*]

[a] *Department of Physics, University of Puerto Rico, San Juan, PR 00931, USA*
[b] *Department of Chemistry, University of Puerto Rico, San Juan, PR 00931, USA*

Received 5 June 2005; accepted 1 August 2005
Available online 29 November 2005

Abstract

The process optimization of nanocrystalline lithium manganate thin films ($Li_xMn_2O_4$; $x = 1.0$–1.4) has been demonstrated by using a cost-effective solution growth technique. Films were first attempted with Pt–Si ($Si/SiO_2/TiO_2/Pt$) substrates but because of inter-diffusion of TiO_2 buffer layer with Pt at higher annealing temperature, phase impure $LiMn_2O_4$ films were obtained. Phase pure films on the basis of XRD analysis were found on Pt substrate at specified growth parameters. The annealing temperature and annealing time were varied, the films annealed at 700 °C for 2 h were found to be the best films. The nanocrystalline nature of the films was revealed by the SEM micrographs and the surface morphology studied using AFM. Finally, the electrochemical properties (cyclic voltammetry and constant current measurements) of these films were analyzed using a home made three-electrode cell and Gamry Battery tester instrumentation. The formation of a prominent layer of fluoride species deposited over the cathode surface during the repeated cycling was revealed by XPS measurements. Further experiments are in progress on identifying the exact composition of these unwanted species. The formation of the Jahn-Teller active Mn^{3+} during electrochemical cycling was completely ruled out from the XPS analysis. Also the very consistent value of $[Mn^{3+}/Mn^{4+}]$ ratio before and after electrochemical cycling on the surface of the film revealed good quality of the films. Finally, the formation of the fluoride layer was concluded as a passive layer that causes the initial capacity drop during first few cycles of the cell performance.

Keywords: Lithium manganate; Nanocrystalline; Cyclic voltammetry

1. Introduction

Lithium manganese oxide based materials are of considerable interest in replacing lithium cobalt oxide as cathode material for Li-ion thin film batteries. However, among wide variety of composition and structural types, the spinel $LiMn_2O_4$ (LMO) based compounds are considered as promising candidates because of their higher abundance, higher voltage output, lower cost, and lower toxicity [1–5]. Most of the work on this material by several groups is in the bulk form [5–8], where the cathode is a composite material consisting of the active material along with the binder (usually PVDF) and conducting carbon. While studies on the bulk materials are favorable for attaining high capacities it is difficult to investigate the fundamental intercalation mechanisms due to composite structure and complicated interface between the cathode and the electrolyte. LMO in thin film form is a suitable choice to overcome these difficulties. Also the widely open issues concerning the capacity fading and attributed mechanisms, such as Jahn-Teller distortion, SEI layer formation, Mn dissolution in electrolyte, etc., can be more precisely studied in thin film form. Another advantage of thin film LMO study will be eventually making an effective all-solid-state microbattery.

Different thin film growth techniques in making LMO thin films, such as electrostatic spray deposition; pulsed laser deposition method, sputtering, and sol–gel method are employed in literatures [9–18]. In vapor deposition technique usually the film is considered to have the same stoichiometry as of the target material. But if the multicomponent target has one or more volatile element present then the stoichiometry control in the film becomes difficult. The solution growth technique, such as sol–gel method is a better technique in dealing these types of difficulties. However, the quality of the thin film is strongly

* Corresponding author. Tel.: +1 787 751 4210; fax: +1 787 764 2571.
E-mail address: rkatiyar@rrpac.upr.clu.edu (R.S. Katiyar).

0378-7753/$ – see front matter © 2005 Elsevier B.V. All rights reserved.
doi:10.1016/j.jpowsour.2005.08.056

dependent on the various preparation conditions and experimental parameters. It is well known that pure spinel $LiMn_2O_4$ is very prone to the capacity fading after repeated electrochemical cycling, which limits its practical use as a potential candidate in commercial Li-ion battery today [19–23]. Many proposed mechanisms were reported in the literature for such degradation. Shin and Manthiram [19] showed that the capacity fading in LMO is due to the development of microstrains and the larger difference in the lattice parameters between the two cubic phases during charging, Chung and Kim [21] showed the onset of Jahn-Teller effect in deeply discharged $Li_xMn_2O_4$ electrodes ($x \sim 1$) with a Mn^{3+} rich region in the surface is the primary cause of the fading. Jang et al. [22] and Xia and Yoshio [23], respectively, showed that the Mn dissolution in the electrolyte and the structural stability in the high voltage region are the causes of the capacity fading. In the present work, we have successfully synthesized good quality phase pure nanocrystalline LMO thin films using a solution growth technique. Both Pt–Si ($Si/SiO_2/TiO_2/Pt$) and platinum substrates were used to make the LMO films under the same experimental parameters. We were unable to get a phase pure film on a Pt–Si substrate, whereas phase pure polycrystalline films were formed on Pt substrate. XRD analysis was used to study the phase formation behavior of all films annealed at different temperatures and time. The surface morphology was studied from the AFM micrograph. The nanocrystalline nature of the films was assigned both from AFM and SEM profiles. Finally, the lithium intercalation and de-intercalation behavior of the films were studied using cyclic voltammetry experiments and further electrochemical studies were done using charge–discharge and cycleability measurements. On the basis of these results the experimental parameters (both growth parameters, annealing time, and annealing temperature) were optimized for high quality LMO films. We carried out the constant current measurements of the optimized LMO film and found there is an initial drop in the capacity during first few cycles of charge–discharge of the cell. We argued that the formation of a dead-layer on the cathode surface is the primary cause of capacity fading. From the XPS results, we concluded that the formation of a passive surface fluoride layer on the electrode surface. The increase in much-debated Jahn-Teller active Mn^{3+} on the surface of the film after electrochemical cycles was discarded from XPS results. However, the exact chemical compositions of the fluoride species had not been identified and further experiment is needed to identify it exactly. A way to find out the composition may give a better understanding of the degradation mechanism.

2. Experimental

Thin films of LMO were synthesized using a chemical solution route. Lithium acetate and manganese acetate (Alfa aeser, 99.99% purity) were used as precursor materials. These were separately dissolved in 2-ethyl hexanoic acid along with chelating agent ethylene glycol to make a transparent and homogeneous sol at temperature ~80 °C. Both sols were mixed together with stirring and slight heating to make 0.5 m/l parent sol. This sol was used to deposit 20 layers of coatings on both $Si/SiO_2/TiO_2/Pt$ and platinum substrates using a spin-coater unit. Each coating was done with ~2000 rpm for 10 s, and after each coating the film was heat treated at 400 °C for 5 min in a furnace in order to remove the organics and other carbon related impurities. This temperature was chosen on the basis of DTA data on our bulk LMO samples where the organic removal undergoes at ~300 °C [24]. Finally, the films were annealed at different higher temperatures (600–850 °C) for different annealing time (1–6 h) in order to crystallize it uniformly. We synthesized $Li_xMn_2O_4$ films of various compositions (with $x = 1.0$, 1.2, and 1.4) under the identical preparation conditions. The XRD analyses of these samples were carried out using Cu Kα radiation from a Seimen D500 diffractometer. The lattice parameters and the crystallite size of the films were determined from the FWHM by deconvoluting the higher angle peaks with a Pearson VII amplitude function in peakfit software. The surface morphology of the process-optimized film was studied using a digital instrument nanoscope AFM and the microstructure was studied using SEM. Both before and after electrochemistry (15 cycles of charge–discharge) the SEM micrographs were recorded. The intercalation and de-intercalation of Li ion into the spinel structure were studied from the cyclic voltammetry experiment. A three-electrode electrochemical cell was fabricated and Gamry software was used to study the electrochemical behavior of the films. The cell consisted of LMO as the working electrode, Li metal as anode, another Li metal as the reference and a liquid electrolyte of ethylene carbonate (EC) and dimethyl carbonate (DMC) in 1:2 ratio. The cycleability of the films was performed using charge–discharge measurements. The X-ray photoelectron spectroscopy spectra were recorded in a PHI 5600 multisystem, using an Al Kα monochromatic source operating at 350 W and 15 kV. The pressure in the main chamber was approximately 6×10^{-10} Torr during the analysis. The survey and the multiplex spectra were obtained with pass energy of 187.85 and 5.85 eV, respectively. The peak-fitting and quantitative evaluation was done with Multipeak V6.1A (Physical Electronics) software. The background was corrected using the Shirley method. All binding energies reported were corrected using the signal for the carbonaceous impurities at 284.5 eV as an internal standard. The change in Mn valence state before and after electrochemistry and surface modification of the film were interpreted from the XPS data.

3. Results and discussion

Due to volatile nature of Li in the compound all of the stoichiometric samples produced extra peaks in the XRD data. These peaks were identified as the Mn_2O_3 peaks. The appearance of these extra peaks were overcome by introducing 20–40% extra Li in the films. Fig. 1 shows the XRD plot of $Li_{1.2}Mn_2O_4$ film grown on $Si/SiO_2/TiO_2/Pt$ substrate. Two samples were taken, one with 15 coatings and the other with 20 coatings prepared under the identical processing conditions. The annealing temperature of 700 °C and annealing time of 2 h were found to represent the optimized conditions for the Pt substrates. But in the case of Pt–Si substrates under these conditions Mn_2O_3 peaks persisted. The appearance of Mn_2O_3 peaks could be due to the

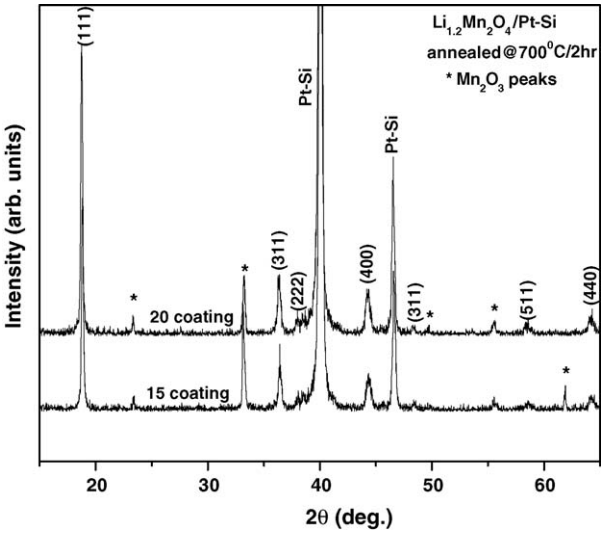

Fig. 1. XRD pattern of $Li_{1.2}Mn_2O_4$ grown on $Si/SiO_2/TiO_2/Pt$ substrate.

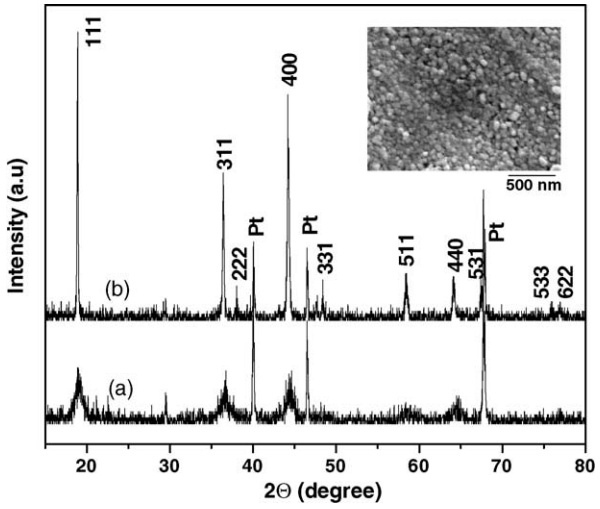

Fig. 3. XRD pattern of (a) as-grown and (b) post-annealed $Li_{1.4}Mn_2O_4$ film on Pt substrate.

interfacial reactions between the lithium and/or manganese with the substrate. The higher annealing temperature with the Pt–Si substrates did not produce better films because of the possible interdiffusion of TiO_2 buffer layer with the Pt top surface of the substrate. Fig. 2 shows the XRD plots of $Li_xMn_2O_4$ films on Pt substrates having different Li concentration ($x = 1.0$, 1.2, and 1.4). It was observed that adding 20% excess Li removed all Mn_2O_3 impurity peaks and showed only the cubic spinel peaks of $LiMn_2O_4$. We also studied the films with 40% excess Li to seek for better electrochemical properties. Several films were synthesized before obtaining these films in order to optimize the experimental parameters for the material. Different annealing temperatures were taken ($T_{ann} = 600$, 700, 800, and 850 °C) and for each of these temperatures four different annealing times ($t_{ann} = 1$, 2, 5, and 10 h) were studied. Based on the XRD and cyclic voltammetry results the films annealed at $T_{ann} = 700$ °C and with the annealing time of $t_{ann} = 2$ h were found to be the most optimized LMO films. Fig. 3 shows the XRD plots of both the as-grown and post-annealed $Li_{1.4}Mn_2O_4$ films. The evolution of spinel peaks even in the as-grown film itself is clearly visible revealing the nanocrystallinity of the films. However, the crystallinity of the as-grown film is poor and upon annealing the FWHM of all the diffracted peaks decreased and intensity increased significantly showing improved crystallinity. The inset in Fig. 3 shows the SEM micrograph of the post-annealed film. It shows that the films are densely packed with grain size of 50–100 nm. Fig. 4 shows the surface morphology of the annealed film taken on a digital instrument nanoscope AFM with a scan size of 618.4 nm and scan rate of 1.969 Hz. The AFM picture also shows similar kind of grain-size distribution.

The electrochemical behavior of all of the films were carried out and on the basis of cyclic voltammetry (CV) and constant-current (charge–discharge) measurements the film with composition $Li_{1.4}Mn_2O_4$, annealed at 700 °C for 2 h was found to yield the best performance. In spinel LMO the Li ions occupy the tetrahedral (8e) sites, Mn ions (in a mixed valence state of Mn^{3+} and Mn^{4+}) occupy the octahedral (16d) sites and O^{2-} ions occupy all the 32e sites and there are 16c vacant sites [25]. These vacant sites serve as reservoirs for extra Li and cause to

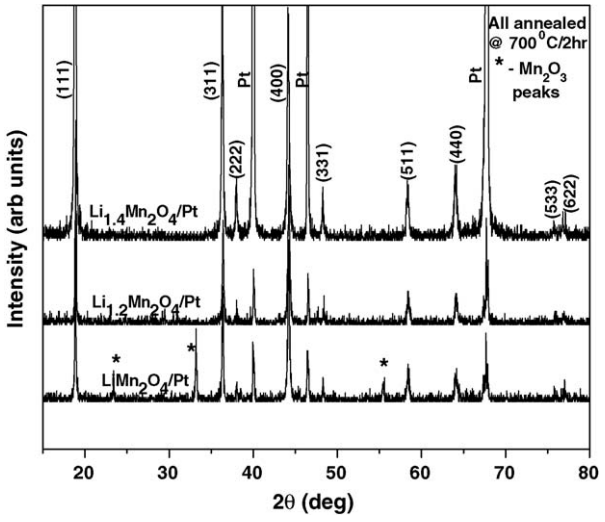

Fig. 2. XRD pattern of $Li_xMn_2O_4$ films on Pt substrates ($x = 1.0$, 1.2, and 1.4).

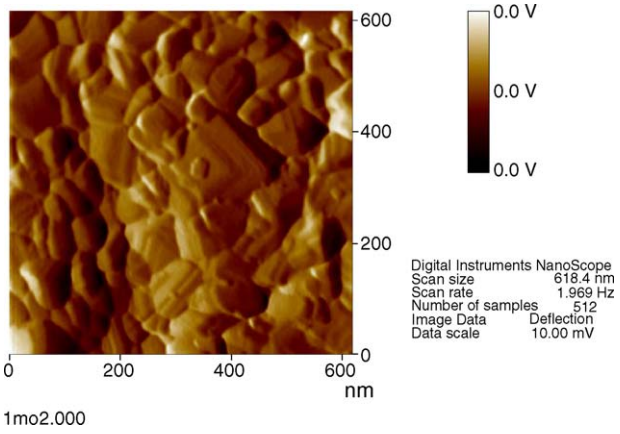

Fig. 4. AFM micrograph of $Li_{1.4}Mn_2O_4$ film.

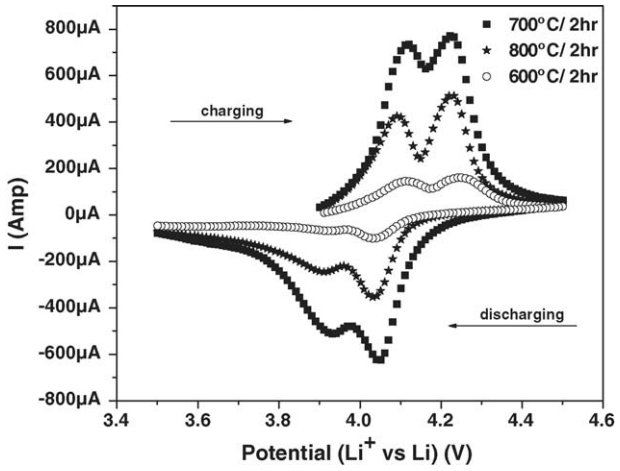

Fig. 5. CV of $Li_{1.4}Mn_2O_4$/Pt film annealed at 600 °C, 700 °C, and 800 °C for 2 h.

overcome the delithiation problem during charge–discharge of the cell and produce an improved cycleability. The possibility of Li segregation is eliminated from the XRD plot (Fig. 3) since no extra phase appears in the pattern. Fig. 5 shows the cyclic voltammetry of $Li_{1.4}Mn_2O_4$/Pt films annealed at 600, 700, and 800 °C, all annealed for 2 h. The measurement was performed in the 4 V range. In all of these films the charging and discharging peaks corresponding to the redox reactions were identified. The appearance of symmetrical CV peaks revealed the reversible Li extraction and insertion processes. In the LMO structure, which is believed to consist of MnO_6 octahedra, each of the octahedra in its opposite corners is shared by LiO_4 tetrahedra. During charging and discharging these Li ions of the shared tetrahedra play the major role in the intercalation process. In a phase pure and stable LMO, the Mn^{3+}/Mn^{4+} ratio is maintained unity by maintaining a balanced $[Mn^{3+}]O_6$ to $[Mn^{4+}]O_6$ octahedra configurations. Both during charging and discharging the appearance of double peaks is the characteristics of the material, indicating that at the first voltage peak (of any one of charging/discharging) half of the Li ion extraction/removal occurs and at the second voltage peak (of any one of charging/discharging) the rest half of Li ion extraction/removal occurs. As revealed from Fig. 5, the corresponding oxidation and reduction peaks of all of the samples fall almost on the same voltage value indicating the intrinsic nature of the LMO spinel material, however the intensity of the peaks varies significantly. Sample annealed at 700 °C for 2 h gives the maximum peak intensity in the CV. This is because of the improved intercalation and de-intercalation of Li^+ ion in the cathode, which is again believed to be related to a stable electrode structure. It is easy to calculate the number of electrons (and hence Li^+ ions transported in the process) from the area under the curve. On the basis of our structural and electrochemical data we confirmed that the $Li_{1.4}Mn_2O_4$/Pt films annealed at 700 °C for 2 h is the process-optimized film. Fig. 6(a and b) shows the film microstructures before and after electrochemistry. Before electrochemistry the film was having comparatively dense particles with particle size 50–100 nm distribution, however upon cycling the film in 4 V range (15 cycles) there were some new porous regions developed on the surface

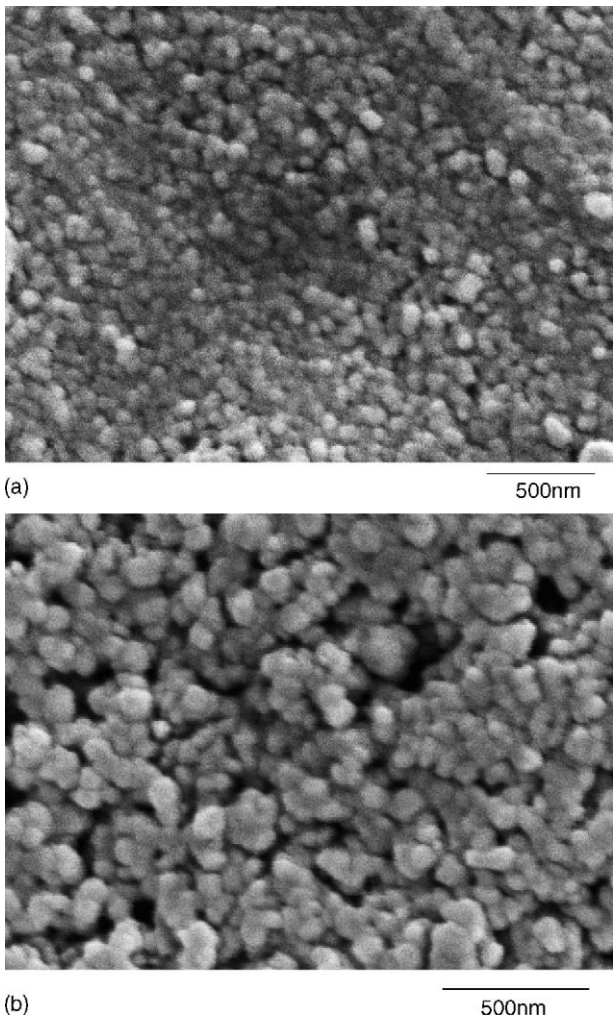

Fig. 6. (a) SEM picture of $Li_{1.4}Mn_2O_4$/Pt film before electrochemical cycling and (b) SEM picture of $Li_{1.4}Mn_2O_4$/Pt film after 15 cycles of charging–discharging cycling.

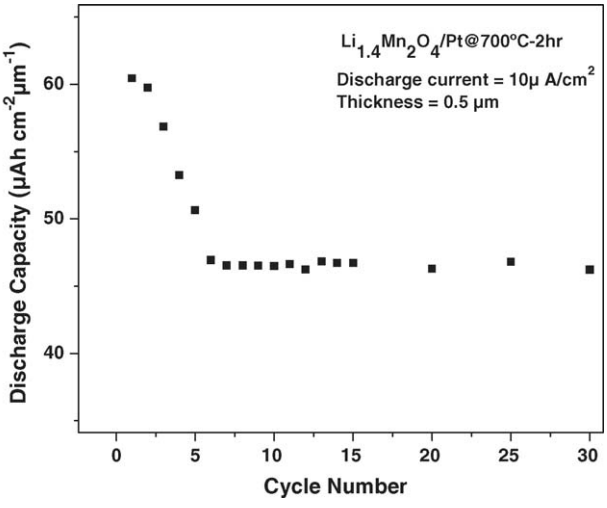

Fig. 7. Cycleability of $Li_{1.4}Mn_2O_4$/Pt film in 4 V range.

Table 1
Comparison of microstructures of $Li_{1.4}Mn_2O_4$/Pt film before and after 15 cycles of charge–discharge

Sample	Lattice parameter '*a*' (Å)	Crystallite size '*t*' (nm)	Lattice strain '*e*'
LMO film before the charge–discharge cycling	8.19387	1.278	0.05662
LMO film after 15 cycles of charge–discharge cycling	8.094	1.880	0.1145

or there was an increase in the formerly existing pore size. This may be related to the dissolution of the electrode material in the electrolyte or the development of strain between the crystallites. To further investigate the nature of the microstructural information after 15 cycles of charging and discharging of the cell we carried out the XRD analysis of the cycled film. Table 1 compares various parameters before and after the charge–discharge cycling. The lattice constant was found to decrease whereas the crystallite size and the lattice strain were found to increase after the electrochemical cycling.

Fig. 7 shows the cycleability of the film in 4 V range performed in a cell having Li anode and EC/DMC electrolyte (1:2, v/v). The constant current measurements were done for 30 cycles. The initial capacity was ~62 μAh cm^{-2} μm^{-1} and after 5–6 cycles it dropped down to ~46 μAh cm^{-2} μm^{-1} after which it remained almost constant. To understand the initial drop in the cell capacity XPS analyses were done on the virgin as well as the cycled film (after 15 cycle). Fig. 8(a–c) shows, respectively, the Mn 2p peak positions of the film before any electrochemical cycling, after 15 cycles of charging and discharging, and 0.7 min of Ar sputtering on the cycled film inside the XPS chamber. The Mn 2p doublets were positioned using Multipeak V6.1A (Physical Electronics) software. The summary of the peak positions and valence states are given in Table 2. The consistent value of $[Mn^{3+}/Mn^{4+}]$ (both peak position ratio and integrated area ratio) before and after electrochemical cycling suggests that there is not much Mn^{3+} formation upon repeated cycling and hence it is not the cause of the initial capacity drop. In Fig. 9, we compare the XPS survey of the LMO film before and after the electrochemical cycling in the whole range of 0–1200 eV. It is evident that there is a number of fluoride species sticking to the surface of the film after it has been cycled in $LiPF_6$/(EC+DMC) electrolyte. During the first few cycles the continuous growth of this layer hinders the Li^+ transport causing the capacity to drop.

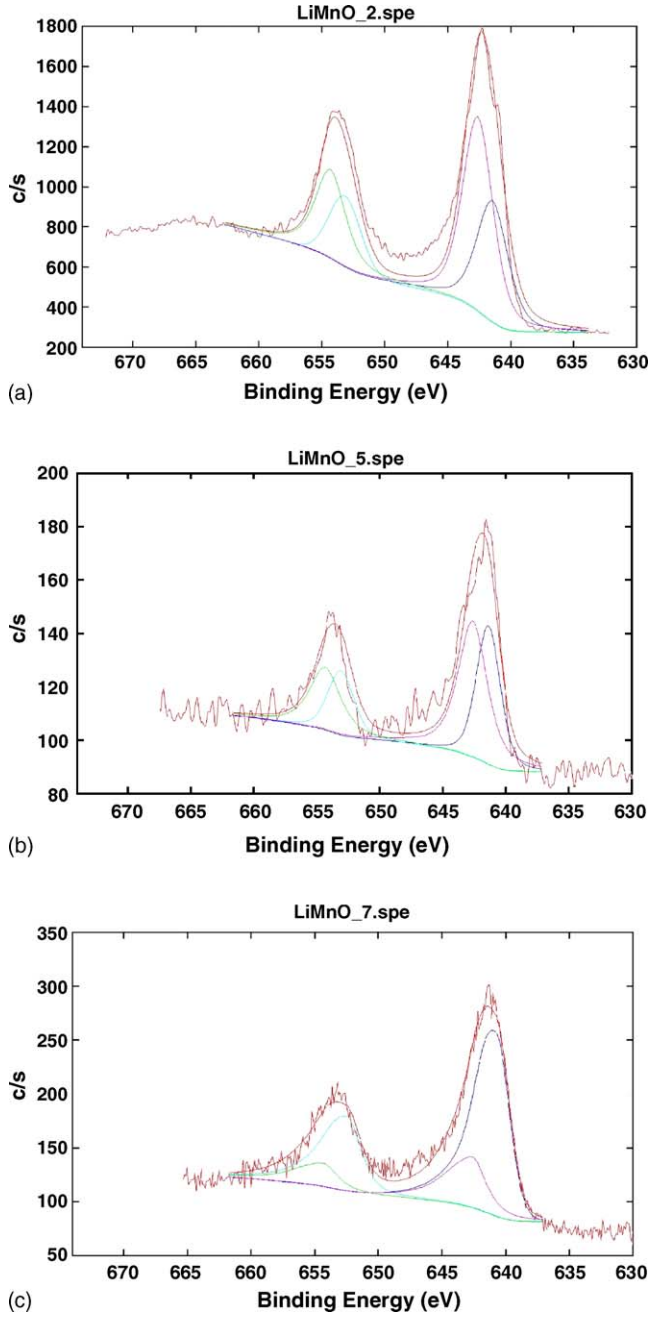

Fig. 8. (a) XPS spectrum of $Li_{1.4}Mn_2O_4$/Pt film showing Mn 2p peak positions before electrochemical cycling, (b) XPS spectrum of $Li_{1.4}Mn_2O_4$/Pt film showing Mn 2p peak positions after 15 cycles of charging–discharging cycles, and (c) XPS spectrum of $Li_{1.4}Mn_2O_4$/Pt film showing Mn 2p peak positions after 15 cycles of charging–discharging cycles with 0.7 min of Ar sputtering.

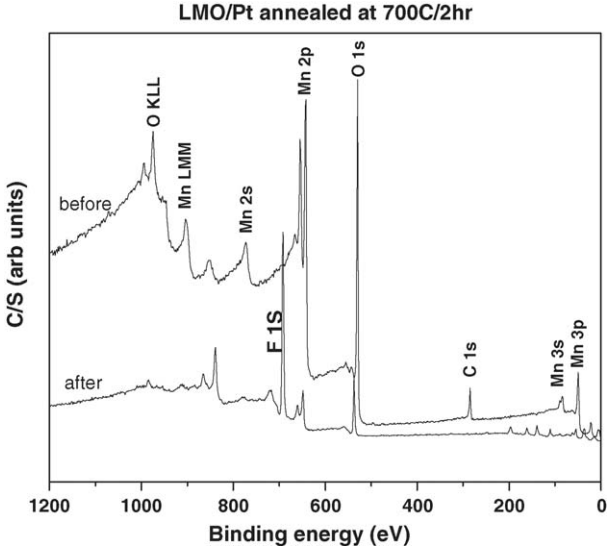

Fig. 9. XPS survey of LMO/Pt film before and after 15 cycles of electrochemical cycling.

Table 2
Summary of XPS analysis of $Li_{1.4}Mn_2O_4$/Pt film before and after 15 cycles of charge–discharge

Sample	Mn^{2+} peak-position (eV)	Mn^{3+} peak-position (eV)	Mn^{4+} peak-position (eV)	Mn^{3+} integrated area (sq. units)	Mn^{4+} integrated area (sq. units)	$[Mn^{3+}/Mn^{4+}]$ peak ratio	$[Mn^{3+}/Mn^{4+}]$ integrated area ratio
LMO before electrochemical cycling	N.A.	641.45	642.61	2283	3555	0.9982	0.64
LMO after 15 cycles (without Ar sputtering)	N.A.	641.38	642.62	145	199	0.9981	0.73
LMO after 15 cycles (with 0.7 min Ar sputtering)	640.79	N.A.	642.59	N.A.	242	N.A.	N.A.

By repeated cycling it has been observed that after few cycles the growth of such a passive layer comes to a saturation value, hence further obstacles for Li^+ transport do not happen. This is reflected in the nearly constant value of the capacity after the initial drop. However, to understand the nature of the passive layer growth and also the nature of its exact composition, in situ measurements are needed.

4. Conclusions

$Li_xMn_2O_4$ in thin film form were grown on various substrates and at various synthesis conditions using solution growth technique. The structural and electrochemical analyses were performed in all of these films. The presence of 20–40% extra Li was required to remove the phase impurity. The as-grown films are nanocrystalline in nature and the crystallinity is improved upon post-annealing. CV peaks correspond to cathodic and anodic reactions corresponding to de-intercalation and intercalation of Li^+ ion. On the basis of the electrochemical data $Li_{1.4}Mn_2O_4$ film annealed at 700 °C for 2 h grown on Pt substrate was found to be the process-optimized film. The cycleability data shows an initial drop during the first few cycles after which it is almost constant. This drop is attributed to the development of a strong passive fluoride layer formation on the surface of the film. The formation of much-debated Jahn-Teller active Mn^{3+} was discarded in our thin film LMO cathodes.

Acknowledgements

The work was partially supported by the grant from DoE (# DE-FG02-01ER45868) and NASA (#NAG3-2676) Glenn research center. XRD and SEM measurements were carried out utilizing the facilities at the UPR Materials Characterization Center (MCC).

References

[1] M.M. Thackeray, W.I.F. David, P.G. Bruce, J.B. Goodenough, Mater. Res. Bull. 18 (1983) 461.
[2] M.M. Thackeray, P.J. Johnson, L.A. de Picciotto, P.G. Bruce, J.B. Goodenough, Mater. Res. Bull. 19 (1984) 179.
[3] J.M. Tarascon, E. Wang, F.K. Shokoohi, W.R. McKinnon, S. Colson, J. Electrochem. Soc. 138 (1991) 2859.
[4] J.M. Tarascon, D. Guyomard, Electrochim. Acta 38 (9) (1993) 1221.
[5] Sun-Ho Kang, J.B. Goodenough, L.K. Rabenberg, Elctrochem. Solid-State Lett. 4 (5) (2001) A49.
[6] S.S. Zhang, T.R. Jow, J. Power Sources 109 (2002) 172.
[7] D.S. Ahn, M.Y. Song, J. Electrochem. Soc. 147 (3) (2000) 874.
[8] P. Lucas, C.A. Angell, J. Electrochem. Soc. 147 (12) (2000) 4459.
[9] D. Shu, K.Y. Chung, W.I. Cho, K.B. Kim, J. Power Sources 114 (2003) 253.
[10] M. Mohamedi, D. Takahashi, T. Itoh, M. Umeda, I. Uchida, J. Electrochem. Soc. 149 (1) (2002) A19.
[11] M. Antaya, K. Cearns, J.P. Preston, J.N. Reimers, J.R. Dahn, J. Appl. Phys. 76 (5) (1994) 2799.
[12] K.A. Striebel, C.Z. Deng, S.J. Wen, E.J. Cairns, J. Electrochem. Soc. 143 (6) (1996) 1821.
[13] K.A. Stribel, E. Sakai, E.J. Cairns, J. Electrochem. Soc. 149 (1) (2002) A61.
[14] N.J. Dudney, J.B. Bates, R.A. Zuhr, S. Young, D.J. Robertson, H.P. Jun, S.A. Hackney, J. Electrochem. Soc. 146 (7) (1999) 2455.
[15] K.F. Chiu, H.H. Hsiao, G.S. Chen, H.L. Liu, J.L. Her, H.C. Lin, J. Electrochem. Soc. 151 (3) (2004) A452.
[16] K. Kushida, K. Kuriyama, Appl. Phys. Lett. 76 (16) (2000) 2238.
[17] Y. Matsuo, R. Kostecki, F. McLarnon, J. Electrochem. Soc. 148 (7) (2001) A687.
[18] Y.H. Rho, K. Knamura, T. Umegaki, J. Electrochem. Soc. 150 (1) (2003) A107.
[19] Y. Shin, A. Manthiram, Electrochem. Solid-State Lett. 5 (3) (2002) A55.
[20] M.Y. Song, D.S. Ahn, H.R. Park, J. Power Sources 83 (1999) 57.
[21] K.Y. Chung, K.-B. Kim, J. Electrochem. Soc. 149 (2002) A79.
[22] D.H. Jang, Y.J. Shin, S.M. Oh, J. Electrochem. Soc. 143 (1996) 2204.
[23] Y. Xia, M. Yoshio, J. Power Sources 66 (1997) 129.
[24] N. Santander, S.R. Das, S.B. Majumder, R.S. Katiyar, Surf. Coat. Technol. 60 (2004) 117–178.
[25] C.M. Julien, M. Massot, J. Phys.: Condens. Matter 15 (2003) 3151.